

Atom-level design strategy for hydrogen evolution reaction of transition metal dichalcogenides catalysts

Sangjin Lee, Sujin Lee, Chaewon Kim and Young-Kyu Han*

Department of Energy and Materials Engineering, Dongguk University-Seoul, Seoul, 04620,
Republic of Korea

*Corresponding Author

E-mail: ykenergy@dongguk.edu

Abstract

Two-dimensional transition metal dichalcogenides are among the most promising materials for water-splitting catalysts. While a variety of methods have been applied to promote the hydrogen evolution reaction on the transition metal dichalcogenides, doping of transition metal heteroatoms have attracted much attention since it provides effective ways to optimize the hydrogen adsorption and H₂ generation reactions. Herein, we provide in-depth and systematic analyses on the trends of the free energy of hydrogen adsorption (ΔG_{H^*}), the most well-known descriptor for evaluating hydrogen evolution reaction performance, in the doped transition metal dichalcogenides. Using the total 150 doped transition metal dichalcogenides, we carried out the atom-level analysis on the origin of ΔG_{H^*} changes upon the transition metal heteroatom doping, and suggest two key factors that govern the hydrogen adsorption process on the doped transition metal dichalcogenides: 1) the changes in the charge of chalcogen atoms where hydrogen atoms adsorbed for the early transition metal doped structures, and 2) the structural deformation energies accompanying in introduced dopants for the late transition metal doped structures. Based on our findings, we interpret from a new perspective how vacancies in the TM-doped TMDs can provide optimal ΔG_{H^*} in HER. We suggest electrostatic control for early TM doped systems and structural control for late TM doped systems as the effective strategies for the thermoneutral ΔG_{H^*} in TMD.

Keywords

Transition metal dichalcogenides, Hydrogen evolution reaction, Water-splitting, Catalyst, First-principles calculation

Introduction

As a sustainable and renewable energy source, hydrogen has attracted tremendous attention and a clean generation of hydrogen has been intensively studied for the last decade. While the demands for hydrogen continue to elevate up to about 24% of the total energy needs until 2050 [1], developing practical and clean hydrogen generation methods from water-splitting is urgent because the hydrogen generation still depends largely on the fossil fuels, producing massive amount of carbon dioxides [2–4]. For hydrogen generation from water, the use of catalyst is considered essential, promoting the hydrogen evolution reaction (HER) with curtailed energy consumption. When designing HER catalysts, the hydrogen adsorption free energy, ΔG_{H^*} , has been considered the most decisive descriptor to predict the hydrogen evolution reaction performance [5–14].

Two-dimensional transition metal dichalcogenides (TMDs) are among the most noteworthy catalyst materials for HER because of their earth abundancy, high stability and controllable electronic structures [15–26]. From the fact that Pt catalysts, the most superior catalysts for HER, show the near-zero ΔG_{H^*} , extensive research efforts have been carried out to design new catalyst materials with thermoneutral ΔG_{H^*} , applying the Sabatier principle in a practical form. In particular, replacing transition metal (TM) of TMD with heteroatoms have been considered promising strategies to optimize the ΔG_{H^*} because doped heteroatoms may promote optimal hydrogen adsorption process and H_2 generation, facilitating the controls of the catalytic activity [27–36]. For examples, Co, Zn, Pd, and Pt were used to reduce the ΔG_{H^*} of MoS_2 by activating their inert basal plane [30–33], and doping of Co, Ni, Cu, and Zn into $MoSe_2$ dragged the high ΔG_{H^*} of non-doped structure into the near-zero values [34–36]. However, although lots of doped TMDs have been demonstrated for enhanced HERs with optimal ΔG_{H^*} , the atomic-scale

understanding of electrostatic and structural changes during the hydrogen adsorption and appropriate general rules explaining the overall relation between the dopant TM and the ΔG_{H^*} have not yet been fully understood.

In this study, we provide the universal trends and underlying atom-level origin observed in the ΔG_{H^*} on the TM doped TMDs. Among TMD materials, MoS₂ has attracted tremendous attention for the last decade as a catalyst for HER and has been extensively studied because of its high stability, low cost, and good performance, and doping of MoS₂ has been one of the major topics to enhance the HER in MoS₂ [28,37–45]. In particular, we pay attention to the stable 2H-MoS₂ phase since it can work as a robust water-splitting catalyst compared to other metastable phases. From the electronic and structural analysis using first-principles calculations on the *3d*, *4d* and *5d* TM doped MoS₂ catalysts, we found that there was a distinctive difference between the early and the late TM dopants with respect to the position of Fermi levels on their *d* bands. While the group 8–12 dopants were expected to show an optimal HER performance with the near-zero ΔG_{H^*} , we revealed that the hydrogen adsorption process in those late TM doped MoS₂ is mainly governed by the structural deformation near the dopant. On the other hand, in the early TM doped MoS₂, a structural deformation is hardly observed but the change in the charge of the chalcogen atom plays a key role to regulate the hydrogen adsorption. We also clarified that both trends were universally valid for other TMD systems (MoSe₂, MoTe₂, CrS₂, and WS₂), where transition metal and chalcogen elements vary. Furthermore, we adapted these findings to verify the role of vacancies in doped TMDs for the optimal ΔG_{H^*} . The chalcogen vacancies in the doped TMDs preliminarily introduce the structural deformation near the dopant even without hydrogen adsorption, then weak Coulomb interaction between adsorbed hydrogen and the late TM dopant leads to the optimal near-zero ΔG_{H^*} . Based on our findings, we provide electrostatic and structural controls as two key

strategies for optimal ΔG_{H^*} , according to the d orbital occupation of metal elements in TMD catalysts, opening a new avenue for improved water-splitting efficiency.

Method

Spin polarized ab initio calculations were performed using density functional theory (DFT) provided in Vienna Ab initio Simulation Package (VASP) [46]. We adopted the Perdew-Burke-Ernzerhof exchange-correlation functionals [47] and projector augmented wave method [48]. The 5×5 supercell structures were prepared for 2H-MoS₂, MoSe₂, MoTe₂, CrS₂, and WS₂ monolayers and relaxed until the Hellmann-Feynman forces were less than -0.02 eV/Å. A 600 eV cutoff energy and a $3 \times 3 \times 1$ Monkhorst k -point mesh were used for all the computations. The obtained lattice parameters for monolayer MX₂ (M = Mo, Cr, and W, and X = S, Se, and Te) were $a = 3.18, 3.32, 3.55, 3.04,$ and 3.19 Å for MoS₂, MoSe₂, MoTe₂, CrS₂, and WS₂, respectively, which are well agreed with previous reports [49–54]. For those five TMD structures, a TM atom (M) was replaced by a dopant transition metal A (A = 3d, 4d, and 5d transition metals) to describe the TM heteroatom doped TMD structures. The free energy of HER reactions (ΔG_{H^*}) was computed for all the 150 doped TMD structures using the equation $\Delta G_{H^*} = \Delta E_H + 0.24$ eV, where ΔE_H is the adsorption energy of a H atom, calculated for $1/2H_2$ at pH = 0 and $p(H_2) = 1$ bar, and the 0.24 eV correction is for the differences in zero-point-energy and entropy [55,56]. A hydrogen atom is attached to a chalcogen atom nearest to the dopant TM. For the cases of the TM doped TMDs with vacancies, a single chalcogen vacancy is placed for the each TMD unit cell at the energetically most stable chalcogen site, which is near the dopant metal atom and a hydrogen atom was adsorbed near the vacancy. The charge for each atom is evaluated using Bader charge analysis [57]. The hydrogen adsorption energy

calculated for a hydrogen atom ($\Delta E_{\text{H_atom}}$) is used for the comparison with the structural deformation energy. The structural deformation energy was evaluated using the equation $\Delta E_{\text{S}} = E_0(\text{TMD}) - E_{\text{S}}(\text{TMD})$, where $E_0(\text{TMD})$ is the energy of the original TMD structure, and $E_{\text{S}}(\text{TMD})$ is computed without ionic relaxation from the doped TMD with an adsorbed hydrogen atom by replacing the dopant atom with the transition metal atom in the original TMD and removing hydrogen [58]. The doping formation energy was evaluated using the equation $\Delta E_{\text{f}} = E(\text{TM:TMD}) - E_0(\text{TMD}) - \mu_{\text{TM}} + \mu_{\text{TM}_0}$, where $E(\text{TM:TMD})$ is the energy of the TM doped TMD, and $E_0(\text{TMD})$ is the energy of the original TMD structure, and μ_{TM} is the energy of a TM atom evaluated for its bulk phase, and μ_{TM_0} is the energy of the original TM atom in its bulk phase. All the atomic structures are illustrated using VESTA code [59].

Results and discussion

2H structures of MoS_2 were prepared with a single TM atom replaced by a dopant TM heteroatom as shown in Figure 1a. We evaluated ΔG_{H^*} , describing the free energy in the hydrogen adsorption process. Figure 1b shows the plots of ΔG_{H^*} for all the doped MoS_2 categorized by *3d*, *4d* and *5d* TM dopants, and the values are listed in Table 1. It is noticeable that there are two evident trends, which include 1) invariant ΔG_{H^*} for early TM dopants (the group 3, 4, and 5 elements), 2) large variation of ΔG_{H^*} for late TM dopants with the maximum at the group 6 dopants, and the minimum near group 10 dopants. Accordingly, the near-zero values of ΔG_{H^*} are observed near the group 9 dopant. It is also noteworthy that ΔG_{H^*} values increase for the group 11 and 12 dopants, approaching zero. These trends in ΔG_{H^*} reaffirm the experimental reports that the late TM doped TMDs showed superior HER performance [27,28,40,45,60–67].

In order to understand the trends in ΔG_{H^*} with respect to the dopant TMs in MoS₂, we analyzed the partial density of states (pDOS) of dopant elements as shown in Figure 2. The *d*-orbitals of dopant TMs have energy gaps between the lower energy states and the higher energy states. The split of *d*-orbitals is attributed to the crystal field under a trigonal prismatic chalcogen coordination in the 2H-TMD structures, where *d*-orbitals of TM split into the higher energy orbitals ($d_{xz}, d_{yz} > d_{xy}, d_{x^2-y^2}$) and the lower energy orbital (d_{z^2}) (Figure 2a) [68–70]. For the early TM dopants (group 3, 4 and 5), the Fermi levels lie in the lower energy bands, which originated from d_{z^2} orbitals (figure 2b-d), while more electrons fill the higher energy bands for the late TMs (Figure 2e-k). The position of the Fermi levels can significantly affect the structural change in hydrogen adsorption process since the attached hydrogen atom will perturb the bonds between the dopant TM and the neighboring sulfur atoms. In the case that the Fermi levels are located in the higher energy states originate under the crystal field from neighboring sulfur atoms, the bond structures near the dopant TM undergoes large structural distortion, directly regulated by the change in the electron filling in the high energy *d*-orbitals.

Figure 3a-j clarify the relation between the Fermi level and the structure deformation when a hydrogen atom is adsorbed. For example, Sc, Ti, V, and Cr doped MoS₂ show little break of the symmetry in the sulfur atoms near the dopant even when a hydrogen atom adsorbed (Figure 3a-d). On the other hand, the dopant atoms largely deviated from their original position and the triangular symmetry of neighboring sulfur atoms is broken when a hydrogen atom adsorbed in Mn, Fe, Co, Ni, Cu, and Zn doped MoS₂. Since the Fermi levels are located in the higher energy bands of these late TM dopants, the adsorbed hydrogen atom will change the electron filling of the higher energy bands, which originate from d_{xz}, d_{yz}, d_{xy} , and $d_{x^2-y^2}$ orbitals, affecting the bond configuration near the TM dopant. The large deformation of the bond symmetry for the

change in higher energy bands is rather inevitable from the fact that the orbitals aligned with the bond from neighboring atoms become unstable, leading to up-shifted energy levels. On the contrary, the change in the lower energy bands have little impact on the bond structure near the dopant atom since down-shifted orbitals have less overlaps with neighboring atoms. The breaking of symmetry near the late TM dopants was also experimentally observed in previous studies [27,71,72]. We found that these relations between the location of Fermi levels and the structural deformation near the dopant atom are generally observed for $4d$ and $5d$ TM dopants as shown in Figure S1 and Figure S2, respectively.

The difference in the structural deformation between the early and late TM doped MoS₂, which is coming from the relative Fermi level position on the TM's d energy states, implies that the hydrogen evolution reactions proceed in a dissimilar manner. As seen in the ΔG_{H^*} curves in Figure 1b, the free energy stays invariant for the early TM dopants while the large variation is observed for the late TM dopants. Figuring out the distinctive behaviors between the early TM dopants and the late TM dopants on ΔG_{H^*} and understanding what factors dominantly determine ΔG_{H^*} , we further analyzed the detailed aspect of hydrogen adsorption on the doped MoS₂. Based on the relatively large variation of ΔG_{H^*} values for the late TM doped MoS₂, we probed a key factor that governing the hydrogen adsorption process near the late TM dopants. Taking the structural deformation observed for all the late TM dopants (Figure 3 and Figure S2) into account, we analyzed the impact of the distortion in the bonds between the dopant and the neighboring chalcogen atoms when a hydrogen atom adsorbed. The distinctive deformation observed in the late TM doped MoS₂ includes a pushed-out TM dopant toward opposite direction to the adsorbed hydrogen atom, invoking one lengthened and two shortened dopant-chalcogen bonds. For example, in the Ni doped MoS₂, which has the largest structural deformation among $3d$ dopants, the lengthened and the shortened Ni–S bonds are 3.19 and 2.23

Å, respectively, originally from the 2.41 Å without the adsorbed hydrogen atom (Figure 3h). Such significant structural deviations in the dopant–neighboring atoms may be attributed to the Coulomb repulsive interaction due to the electric charge of the dopant and the adsorbed hydrogen atom. However, the electric charges of the late TM dopants were lower than those of the early transition metal dopants in general, and the charge of the adsorbed hydrogen atoms is somewhat less positive compared to the early TM doped cases (Figure S3), indicating charge interaction is not predominant in HER on the late TM doped TMDs. The lower positive charges in the late TM dopants than those in the early TM dopants may originate from the decreased difference in the electronegativity between the late TM dopants (1.6–2.4) and sulfur (2.6). The electronegativity of early TM is in the range of 1.2–1.6.

Instead, we focused on the structural deformation energies shown in the late TM doped MoS₂. Taking the relations between the Fermi level and the asymmetry in the dopant–neighboring bonds from the distorted crystal fields into account, we analyzed how effectively the late TM doped TMDs optimize their structure when a hydrogen atom adsorbed using the deformation energies. Figure 4 shows comparison between the hydrogen adsorption energy ($\Delta E_{\text{H_atom}}$) and the structural deformation energy (ΔE_{s}) for 3*d*, 4*d*, and 5*d* TM doped MoS₂. Note that $\Delta E_{\text{H_atom}}$ is evaluated for the hydrogen atom, which is shifted from ΔG_{H^*} by the same amount of energy ($\Delta E_{\text{H_atom}} = \Delta G_{\text{H}^*} - 2.49$ eV) since the difference is only from the reference energy (H₂) and the entropic contribution. We adopted $\Delta E_{\text{H_atom}}$ for this analysis to clearly show the relations between the hydrogen adsorption and the structural deformation in the doped TMD catalyst. The structural deformation energy is evaluated as an energy difference between the doped TMD structure with and without the adsorbed hydrogen atom, where the dopants were replaced by the original TMD elements and the adsorbed hydrogen atom was not considered in order to evaluate contributions solely from the structural change. Note that the structural deformation

energy is negligible for the early TM doped MoS₂ because no significant structural distortion is observed for them. However, very interestingly, the trends of the structural deformation energies agree well with those of the ΔE_{H_atom} for the late TM doped MoS₂ (Figure 4), indicating that the structural distortion and relaxation predominantly regulate the hydrogen adsorption on the late TM doped MoS₂. The strong correlation between the ΔE_{H_atom} and ΔE_s trends can be understood in terms of the extent to which the doped TMD structures are energetically stabilized by the adsorbed hydrogen atom. As shown in Figure 5, the doping formation energy in the late TM doped MoS₂ and the structural deformation energy (Figure 4) have noticeably similar trends with the opposite sign, implying that the breaking of the centrosymmetry caused by hydrogen adsorption effectively alleviate the accumulated energy into TMDs from TM heteroatom doping. It should be mentioned that Hg doped MoS₂ shows somewhat unstable doped TMD structures where a Hg dopant largely deviates from the TM metal position in the original TMD, leading to the unusually high doping formation energy (Figure S4). The closely correlated trends between the structural deformation and the hydrogen adsorption suggest that ΔG_{H^*} can be readily tweaked by controlling the distortion of the local structure around the dopants.

Understanding a general role of dopant TM heteroatoms in TMD catalysts, we expanded our computations to other TMD materials and checked if the trends in ΔG_{H^*} observed in TM doped MoS₂ were generally valid. We evaluated ΔG_{H^*} for MoSe₂ and MoTe₂ where S in MoS₂ changed to the heavier chalcogen elements, and CrS₂ and WS₂ where Mo in MoS₂ changed to the 3*d* and 5*d* transition metal in the same group 6. As shown in Figure 6, the trends in ΔG_{H^*} for MoSe₂, MoTe₂, CrS₂, and WS₂ are similar to those for MoS₂, implicating our discussion for ΔG_{H^*} in the TM doped MoS₂ should be valid for the other TMD catalysts. In fact, we observed that the relation between the position of Fermi levels with respect to *d* orbitals of TM dopants

and the symmetry breaking near the dopant when a hydrogen adsorbed was also very similar to the case of MoS₂ (Figure S5–S8). Moreover, the analogous trends in the structural deformation energy with the hydrogen adsorption energy shown in the late TM doped MoS₂ were also confirmed in the late TM doped MoSe₂, MoTe₂, CrS₂, and WS₂ (Figure S9–S12).

On the other hand, for the case of early TM dopants, relatively invariant ΔG_{H^*} values are observed for the case of early TM dopants within each TMD, whereas different TMDs show dissimilar ΔG_{H^*} . For examples, ΔG_{H^*} for Sc, Ti, and V doped MoS₂ are 0.29, 0.39, and 0.32 eV, respectively, which is substantially lower than those for MoSe₂ (0.73, 0.76, and 0.78 eV for Sc, Ti, and V dopant, respectively). The largest ΔG_{H^*} are observed for those early TM dopants in MoTe₂ (0.89, 0.84, and 0.94 eV for Sc, Ti, and V dopant, respectively). These differences in ΔG_{H^*} values seem to originate from the chalcogen atoms (S, Se, and Te) where the charge transfer may occur with adsorbed H atoms. It is worth noting that there is a positive correlation between ΔG_{H^*} and the change in charge of the H-adsorbed chalcogen atom, as seen in Figure 7a. Considering negligible structural deformation observed for H adsorption, it can be inferred that the hydrogen adsorption energy for these early TM doped TMDs may mainly result from the charge transfer between hydrogen atom and the chalcogen atom. When a hydrogen atom adsorbed on the early TM doped TMDs in the HER process, charge transfer occurs between the hydrogen atom and TMDs, acting on lower energy states of the dopant TM atom. While changes in the lower energy states of the dopant TM have little impact on the structural deformation, the hydrogen adsorption energy is dominantly affected by the charge redistribution determined by the electronegativity of chalcogen atoms. It is also noteworthy that there is no noticeable relation between the charge transfer and ΔG_{H^*} in the late TM doped TMDs as plotted in Figure 7b. For the early TM dopant, therefore, electrostatic control near the chalcogen atom where a hydrogen adsorbed is a key strategy for regulating ΔG_{H^*} in TMD

catalysts.

Using the key findings governing HER on doped TMDs, the role of vacancy in the doped MoS₂ catalysts for HER can be also explained. While introducing vacancies into the TMD catalysts has been considered an effective strategy for optimizing ΔG_{H^*} and enhancing HER performance [25,73–76], extensive analyses in atomic-scale have not been yet provided enough for the ΔG_{H^*} optimization. As shown in the ΔG_{H^*} evaluation for the doped MoS₂ with a sulfur vacancy (Figure 8a), most of the late TM doped MoS₂ show the optimized ΔG_{H^*} with near-zero values, indicating that well-balanced hydrogen adsorption and desorption process occur in the MoS₂ with vacancies in contrast to the case of pristine MoS₂ without vacancies where a relatively large variation in ΔG_{H^*} was observed. Note that the early TM doped MoS₂ catalysts with sulfur vacancies do not show the near-zero ΔG_{H^*} values, showing the similarly invariant ΔG_{H^*} as in the non-vacancy cases since there is no participation of the structural deformation. In other words, vacancies in the doped MoS₂ successfully alleviate the impact of structural deformation upon hydrogen adsorption which critically governed the ΔG_{H^*} in the non-vacancy cases. We confirmed that the deformation of near-dopant structures, which is the breaking of the triangular centro-symmetry, in the doped MoS₂ when a hydrogen adsorbed were similarly seen in the doped MoS₂ with vacancies before hydrogen adsorption. For example, as seen in Figure 8b, the dopant in the Ni-doped MoS₂ is pushed-out even without an adsorbed hydrogen atom when a sulfur vacancy exists. Note that the aspect of TM dopant shift is in a similar manner with Figure 3h, which includes the pushed-out TM dopant leaving two-shortened TM–S bonds and the widened vacancy space. From the role of structural deformation in HER as discussed in the case of no vacancy, it is inferred that the stabilization of the doped MoS₂ structures via TM dopant shift occurs preliminarily to the hydrogen adsorption solely by introducing sulfur vacancies. Meanwhile, ΔG_{H^*} in the case of no structural deformation from

hydrogen adsorption become sensitive to the charge interactions as analyzed in the early TM doped MoS₂ cases. In particular, the relative low charge of late TM dopant and the increased distance between the late TM dopant and the adsorbed hydrogen atom from the structural deformation may result in the weak Coulomb interactions upon hydrogen adsorption, leading to the optimal ΔG_{H^*} values. The Bader charge of the early and late TM dopants are 1.28–1.76 e and 0.10–1.25 e (Figure S13), respectively, and the distance between TM dopant and adsorbed hydrogen atom is 2.34–3.23 Å in late TM dopants, which is much longer than those in early TM dopants (2.15–2.42 Å) due to the structural deformation from vacancies (Figure S14). As shown in Figure 8c, ΔG_{H^*} and Coulomb interactions are strongly related in the TM doped MoS₂ with vacancies, confirming that weak Coulomb interactions correspond to near-zero ΔG_{H^*} in the late TM doped cases. The relations between ΔG_{H^*} and Coulomb interactions in addition to the detailed structural deformation in the late TM doped MoS₂ with vacancies were also applicable to other TMDs as shown in Figure S15-S18.

Although we rationalized the role of vacancies in the doped MoS₂ for HER using the two governing factors and explained how those factors effectively optimized the ΔG_{H^*} in the late TM doped cases, adopting vacancies into TMDs is not advantageous for catalytic activities in various aspects. It is known that the vacancies in TMDs may reduce the structural and chemical stability of TMD due to the vacancy clustering [77,78] and the oxidation of chalcogen vacancies [79,80], which may lead to the degradation of HER performance. In addition to the estimation of individual methods for the enhanced performance as HER catalysts in atom-level, and assessment of the strategies in terms of the scope of efficacy, our findings can suggest effective ways to achieve the thermoneutral ΔG_{H^*} specifically for both the early and late TM dopants, providing a practical guideline for probing new TMD based catalysts. For the early TM dopants, electrostatic control of the hydrogen adsorption site is the key strategy since the

charge transfer in the chalcogen near the dopant regulates the hydrogen adsorption process. Although the single doping of the early TM showed the non-near-zero ΔG_{H^*} , tuning the charge of the chalcogen atoms, for example, by increasing the number of dopant TM atoms near the hydrogen adsorption site, doping into the chalcogen sites, adding non-TM atoms that transferring charges on TMDs, and developing heterostructures for charge transfer with TMDs may help optimize the ΔG_{H^*} of TMD materials. On the other hand, for the late TM dopants, local structural control can promote HER providing the near-zero ΔG_{H^*} . Since the breaking of the symmetry near the dopant TM regulate the stability of the hydrogen adsorbed TMD structures, the use of substrates adjusting the structural deformation, adopting the strain into the TMD layers for the tailored dopant-chalcogen distances, using composite structures for the controlled deformation from mismatch, and the doping of multiple types of TM atoms for the tuning of the local structural distortion may provide feasible access to the optimal ΔG_{H^*} .

Conclusions

The HER performance of the *3d*, *4d* and *5d* TM doped TMD was evaluated using ΔG_{H^*} on MoS₂ based catalysts. We revealed that the chemical bond structures between dopant and its neighboring chalcogen atoms when a hydrogen atom adsorbed were regulated by the Fermi level position at the dopant *d* bands. In the case of the early TM doped MoS₂, ΔG_{H^*} is related to the change in the charge of the chalcogen atom where a hydrogen atom adsorbed, and no structural deformation is observed. On the other hand, the late TM doped MoS₂ undergo a significant structural deformation where the displacement of dopant TM determines how effectively the adsorbed hydrogen stabilize the TMD structures. We verified these trends were generally valid in other TMDs such as MoSe₂, MoTe₂, CrS₂, and WS₂. Using the TM dopants'

role we found, we could provide rational explanation on the role of vacancies for the optimal ΔG_{H^*} in the late TM doped MoS₂. We suggested that the electrostatic and structural controls near the active sites in TMD catalysts play a key role in achieving the thermoneutral ΔG_{H^*} , and the use of those strategies can be expanded to other TMD materials than the TMD systems considered in this work. Using the relative position between the *d*-band energy states of a dopant TM and Fermi level which is determined by the energy states of TM in TMD, it can be decided which control should be adopted for the dopant. If the strategies for the optimal ΔG_{H^*} is appropriately selected from among electrostatic controls and the structural controls, the efficiency of material development can be maximized. Considering the intensive attention to the TMD materials as a promising HER catalyst, the two key strategies we suggested can help design a new TMD catalysts for the superior water-splitting capability with enhanced HER performance.

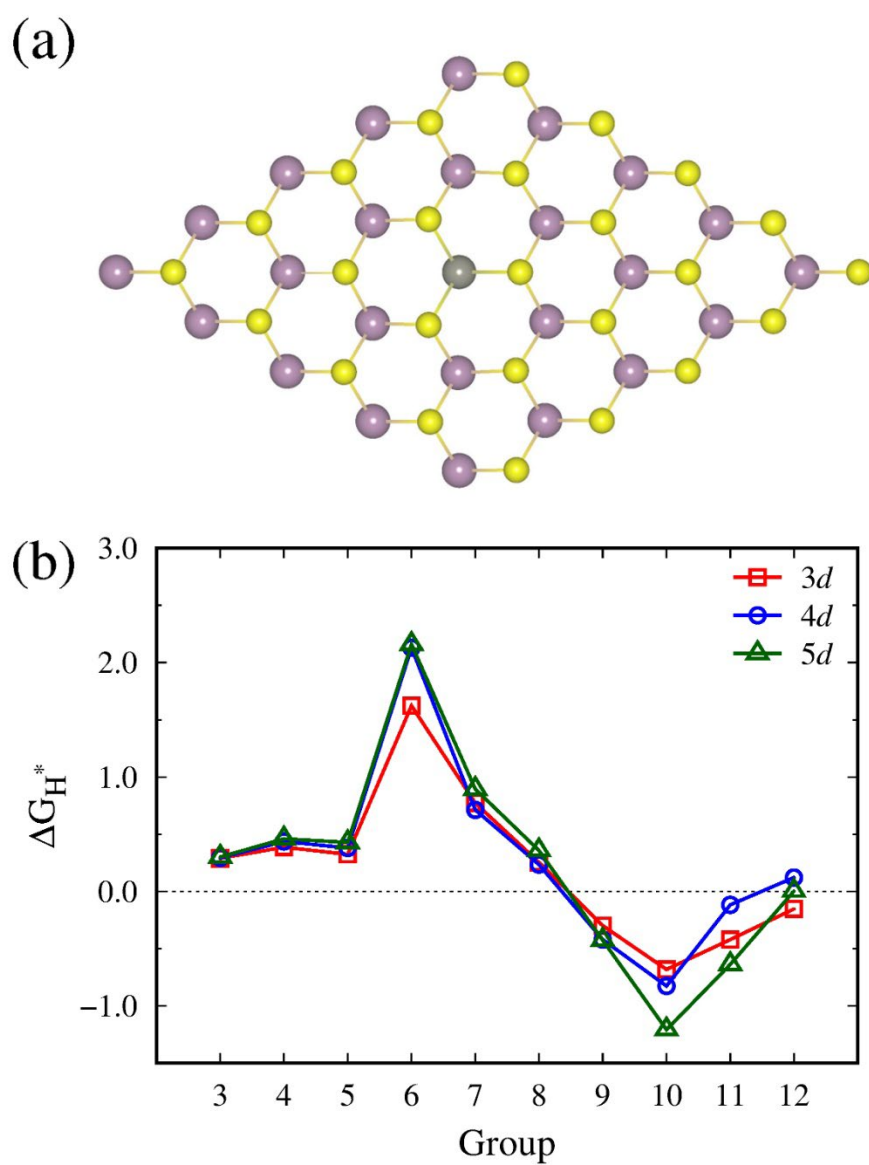


Figure 1. (a) An example structure of TM heteroatom doped TMDs, where purple, yellow and grey spheres represent Mo, S and dopant TM, respectively. (b) ΔG_{H^*} for $3d$, $4d$, and $5d$ TM doped MoS_2 .

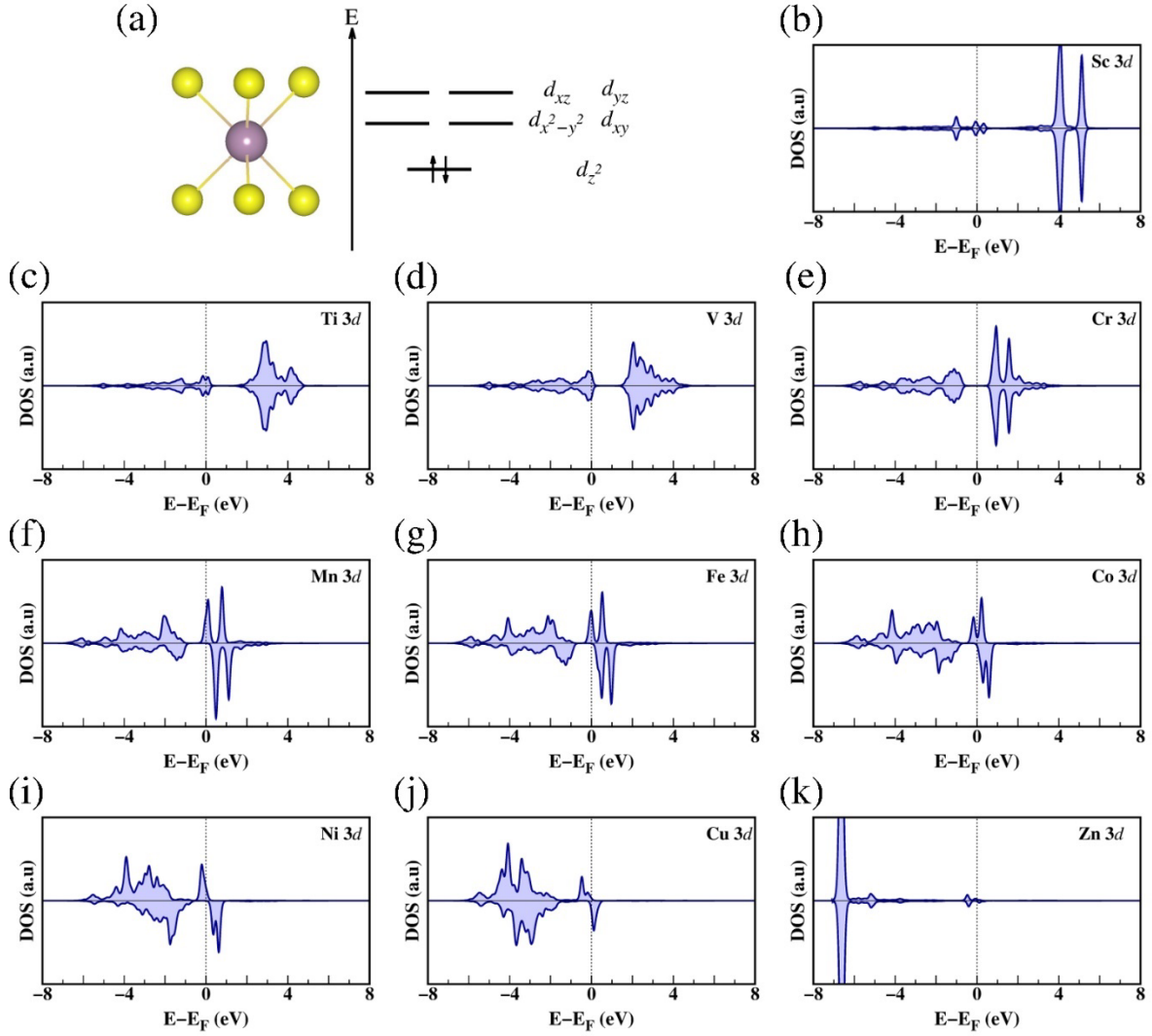


Figure 2. (a) A trigonal prismatic structure of 2H-TMDs (left) and d band alignment of TM under the crystal field from chalcogen atoms (right). Partial density of states of 3d band of a dopant TM in the TM, (b) Sc, (c) Ti, (d) V, (e) Cr, (f) Mn, (g) Fe, (h) Co, (i) Ni, (j) Cu, and (k) Zn, doped MoS₂.

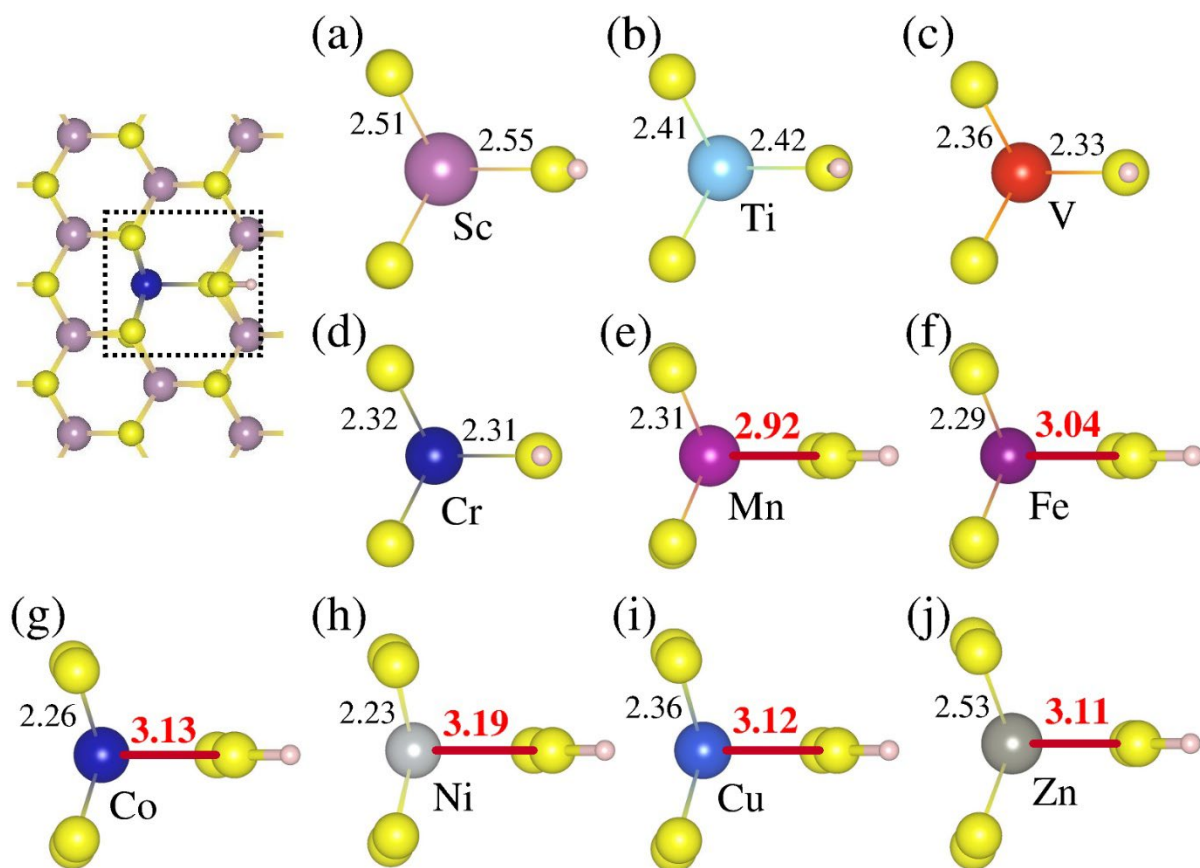


Figure 3. Structures of the TM doped MoS₂ when a hydrogen atom adsorbed. The purple, yellow, and pink spheres represent Mo, S and H atom, respectively, and the bond lengths (Å) are marked for dopant-chalcogen bonds. The triangular centro-symmetry near the dopant is maintained in early TM doped MoS₂ (a-d) and broken in late TM doped MoS₂ (e-j).

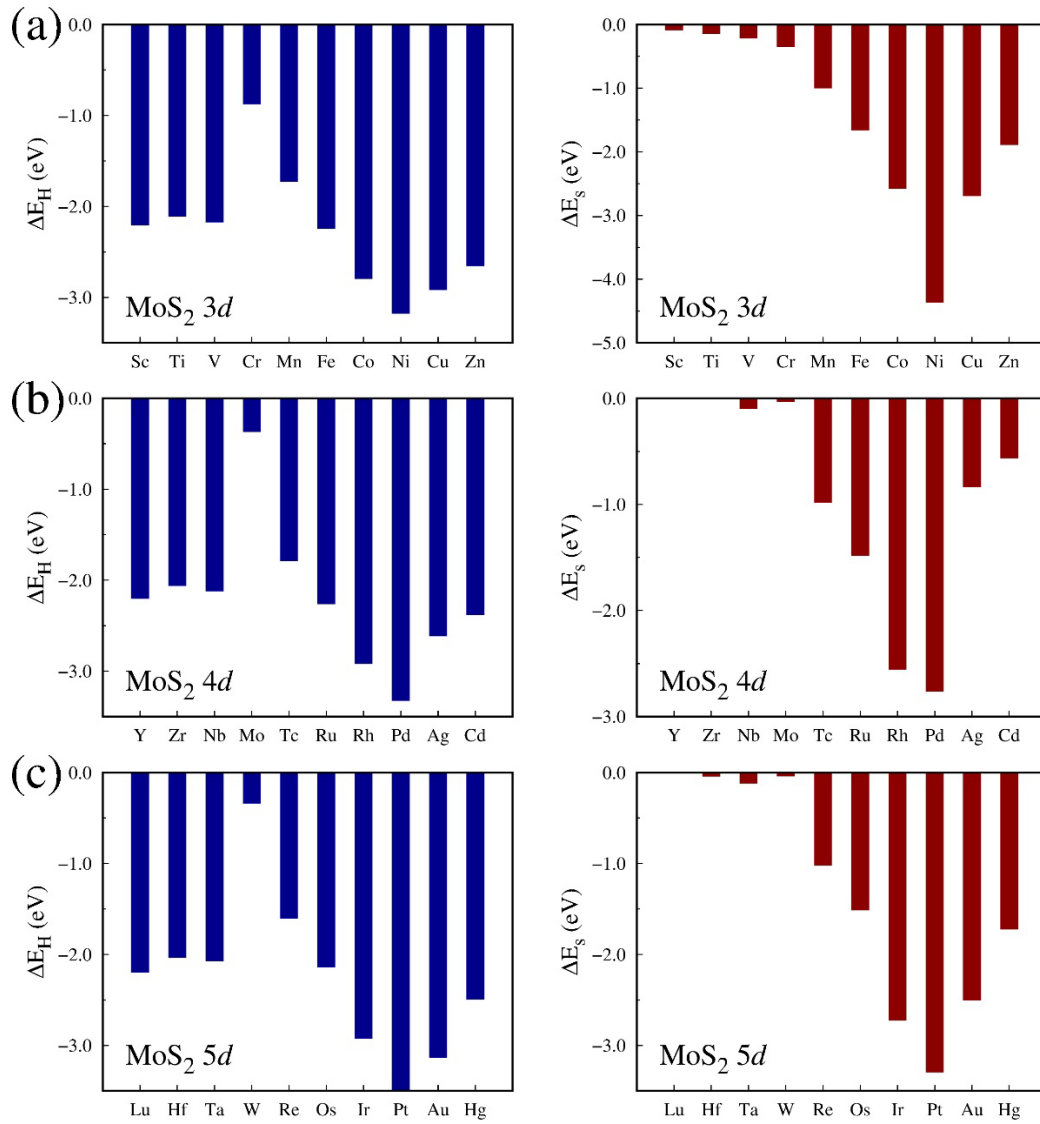


Figure 4. Comparisons between the hydrogen adsorption energy (ΔE_{H_atom}) and the structural deformation energy (ΔE_s) for (a) 3d, (b) 4d, and (c) 5d TM doped MoS₂.

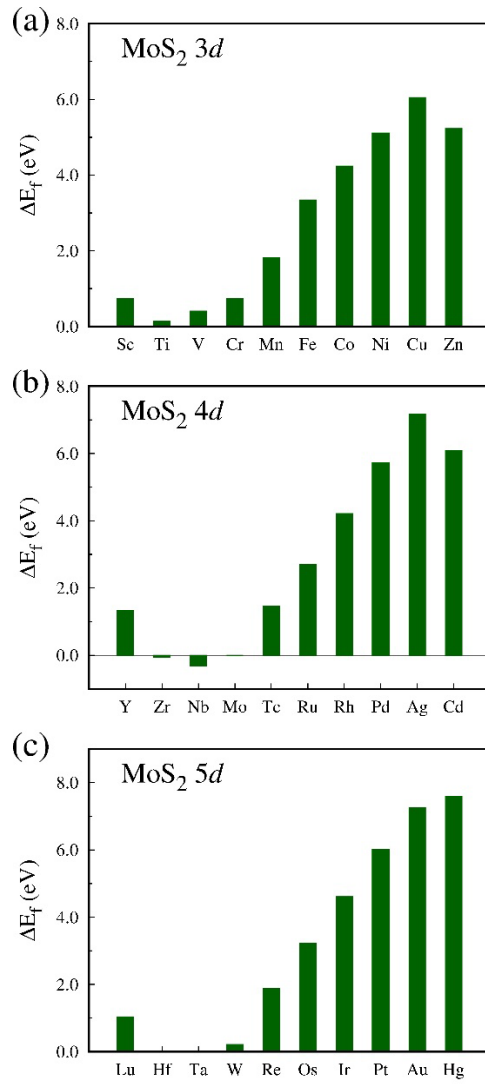


Figure 5. The doping formation energy (ΔE_f) for (a) 3d, (b) 4d, and (c) 5d TM doped MoS_2 .

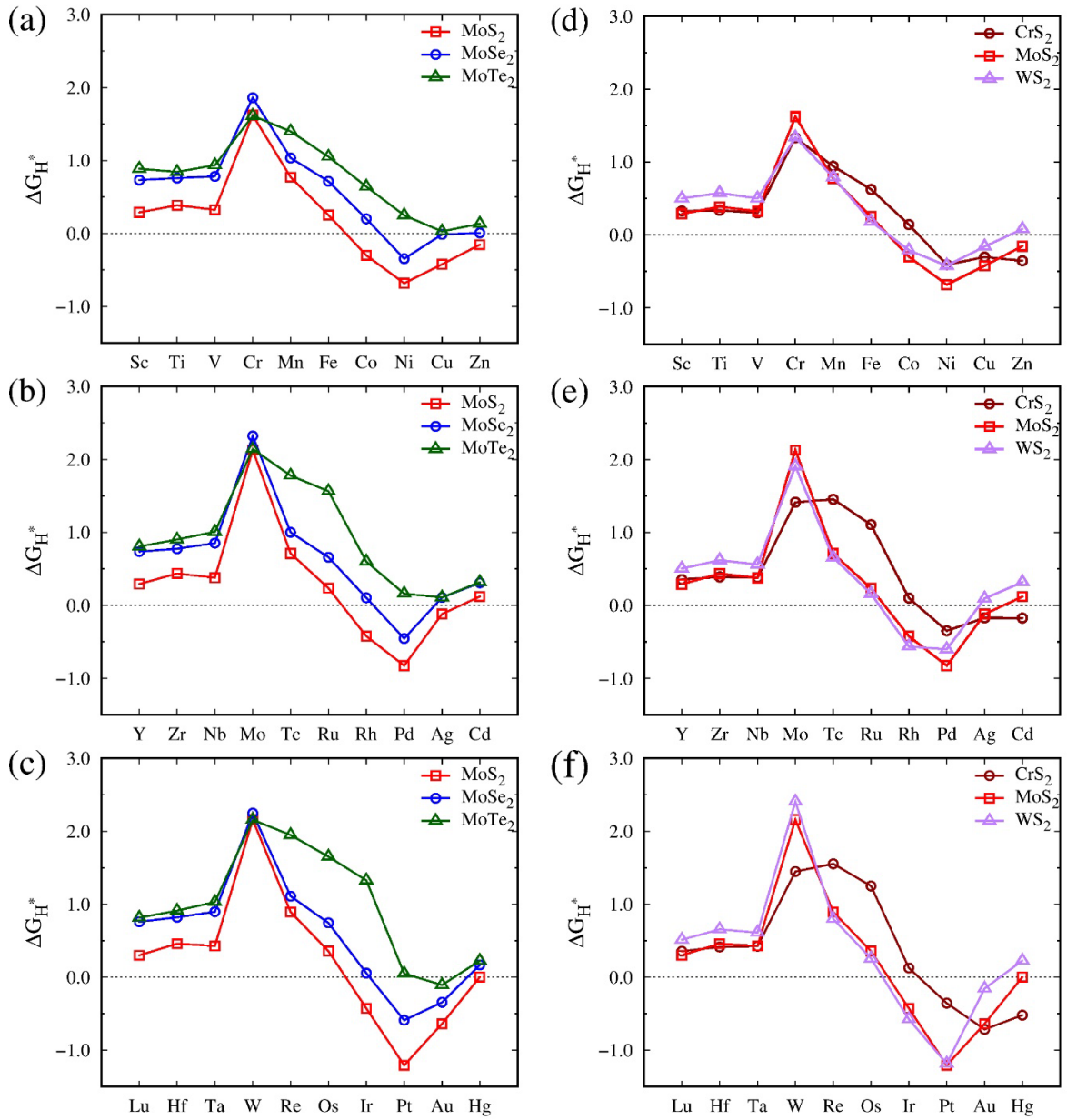


Figure 6. ΔG_{H^*} for (a) 3d, (b) 4d, and (c) 5d TM doped MoS₂, MoSe₂, and MoTe₂, and ΔG_{H^*} for (e) 3d, (e) 4d, and (f) 5d TM doped CrS₂, MoS₂, and MoTe₂.

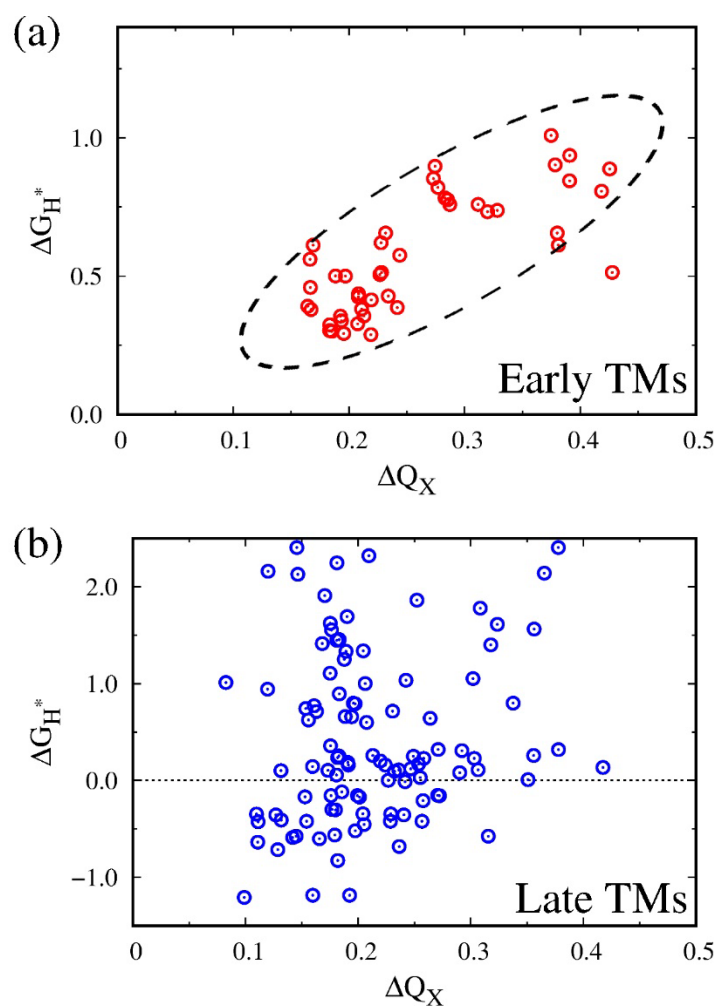


Figure 7. Relations between ΔG_{H^*} and the changes in charge of chalcogen atom when a hydrogen adsorbed (ΔQ_X) for (a) early TM and (b) late TM doped TMDs. ΔQ_X is the difference in the Bader charges of the chalcogen atom before and after the hydrogen adsorption.

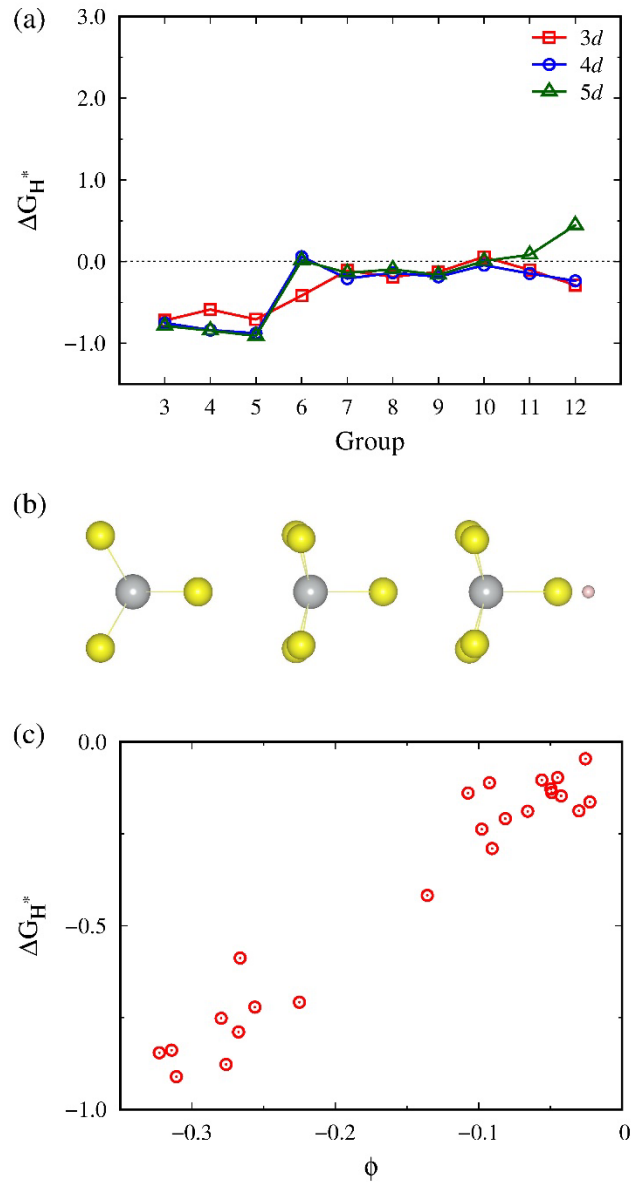


Figure 8. (a) ΔG_{H^*} for 3d, 4d, and 5d TM doped MoS₂. (b) Structures of Ni doped MoS₂ without vacancies (left), with vacancies (center) before hydrogen adsorption, and with vacancies (right) after hydrogen adsorption. The purple, yellow, grey, and pink spheres represent Mo, S, Ni and H atoms, respectively. (c) Relations between ΔG_{H^*} and the Coulomb interaction (ϕ) between the TM dopant and the adsorbed hydrogen atom. The Coulomb interaction is evaluated using the Bader charges of the dopant and hydrogen atom, and their distance.

Table 1. ΔG_{H^*} (eV) of 3*d*, 4*d* and 5*d* TM doped MoS₂ monolayer structures.

3 <i>d</i>	ΔG_{H^*}	4 <i>d</i>	ΔG_{H^*}	5 <i>d</i>	ΔG_{H^*}
Sc	0.29	Y	0.29	Lu	0.30
Ti	0.39	Zr	0.44	Hf	0.46
V	0.32	Nb	0.38	Ta	0.43
Cr	1.62	Mo	2.13	W	2.16
Mn	0.77	Tc	0.71	Re	0.89
Fe	0.25	Ru	0.24	Os	0.36
Co	-0.30	Rh	-0.42	Ir	-0.43
Ni	-0.68	Pd	-0.83	Pt	-1.21
Cu	-0.42	Ag	-0.12	Au	-0.64
Zn	-0.15	Cd	0.12	Hg	0.00

References

- [1] D.A. Cullen, K.C. Neyerlin, R.K. Ahluwalia, R. Mukundan, K.L. More, R.L. Borup, A.Z. Weber, D.J. Myers, A. Kusoglu, New roads and challenges for fuel cells in heavy-duty transportation, *Nat. Energy*. 6 (2021) 462–474.
- [2] C. Kemfert, F. Präger, I. Braunger, F.M. Hoffart, H. Brauers, The expansion of natural gas infrastructure puts energy transitions at risk, *Nat. Energy*. 7 (2022) 582–587.
- [3] C.E. Finke, H.F. Leandri, E.T. Karumb, D. Zheng, M.R. Hoffmann, N.A. Fromer, Economically advantageous pathways for reducing greenhouse gas emissions from industrial hydrogen under common, current economic conditions, *Energy Environ. Sci*. 14 (2021) 1517–1529.
- [4] S. van Renssen, The hydrogen solution?, *Nat. Clim. Chang*. 10 (2020) 799–801.
- [5] Z.W. She, J. Kibsgaard, C.F. Dickens, I. Chorkendorff, J.K. Nørskov, T.F. Jaramillo, Combining theory and experiment in electrocatalysis: Insights into materials design, *Science*. 355 (2017).
- [6] C. Hu, H. Liu, Y. Liu, J.F. Chen, Y. Li, L. Dai, Graphdiyne with tunable activity towards hydrogen evolution reaction, *Nano Energy*. 63 (2019) 103874.
- [7] Y. Qiao, P. Yuan, C.W. Pao, Y. Cheng, Z. Pu, Q. Xu, S. Mu, J. Zhang, Boron-rich environment boosting ruthenium boride on B, N doped carbon outperforms platinum for hydrogen evolution reaction in a universal pH range, *Nano Energy*. 75 (2020) 104881.
- [8] T. Ling, T. Zhang, B. Ge, L. Han, L. Zheng, F. Lin, Z. Xu, W.-B. Hu, X.-W. Du, K. Davey, S.-Z. Qiao, Well-Dispersed Nickel- and Zinc-Tailored Electronic Structure of a Transition Metal Oxide for Highly Active Alkaline Hydrogen Evolution Reaction, *Adv. Mater*. 31 (2019) 1807771.
- [9] T. Liu, P. Diao, Z. Lin, H. Wang, Sulfur and selenium doped nickel chalcogenides as efficient and stable electrocatalysts for hydrogen evolution reaction: The importance of the dopant atoms in and beneath the surface, *Nano Energy*. 74 (2020) 104787.
- [10] D. Liu, X. Li, S. Chen, H. Yan, C. Wang, C. Wu, Y.A. Haleem, S. Duan, J. Lu, B. Ge, P.M. Ajayan, Y. Luo, J. Jiang, L. Song, Atomically dispersed platinum supported on curved carbon supports for efficient electrocatalytic hydrogen evolution, *Nat. Energy*. 4 (2019) 512–518.
- [11] W. Liu, X. Wang, F. Wang, K. Du, Z. Zhang, Y. Guo, H. Yin, D. Wang, A durable and pH-universal self-standing MoC–Mo₂C heterojunction electrode for efficient hydrogen evolution reaction, *Nat. Commun*. 12 (2021) 6776.
- [12] Z. Li, J.Y. Fu, Y. Feng, C.K. Dong, H. Liu, X.W. Du, A silver catalyst activated by stacking faults for the hydrogen evolution reaction, *Nat. Catal*. 2 (2019) 1107–1114.
- [13] E. Skúlason, V. Tripkovic, M.E. Björketun, S. Gudmundsdóttir, G. Karlberg, J. Rossmeisl, T. Bligaard, H. Jónsson, J.K. Nørskov, Modeling the electrochemical hydrogen oxidation and evolution reactions on the basis of density functional theory calculations, *J. Phys. Chem. C*. 114 (2010) 18182–18197.

- [14] J.K. Nørskov, T. Bligaard, A. Logadottir, J.R. Kitchin, J.G. Chen, S. Pandalov, U. Stimming, Trends in the Exchange Current for Hydrogen Evolution, *J. Electrochem. Soc.* 152 (2005) J23.
- [15] L. Lin, P. Sherrell, Y. Liu, W. Lei, S. Zhang, H. Zhang, G.G. Wallace, J. Chen, Engineered 2D Transition Metal Dichalcogenides—A Vision of Viable Hydrogen Evolution Reaction Catalysis, *Adv. Energy Mater.* 10 (2020) 1903870.
- [16] Q. Wang, Y. Lei, Y. Wang, Y. Liu, C. Song, J. Zeng, Y. Song, X. Duan, D. Wang, Y. Li, Atomic-scale engineering of chemical-vapor-deposition-grown 2D transition metal dichalcogenides for electrocatalysis, *Energy Environ. Sci.* 13 (2020) 1593–1616.
- [17] I.S. Kwon, I.H. Kwak, G.M. Zewdie, S.J. Lee, J.Y. Kim, S.J. Yoo, J.G. Kim, J. Park, H.S. Kang, MoSe₂–VSe₂–NbSe₂ Ternary Alloy Nanosheets to Boost Electrocatalytic Hydrogen Evolution Reaction, *Adv. Mater.* 34 (2022) 2205524.
- [18] Q. Fu, J. Han, X. Wang, P. Xu, T. Yao, J. Zhong, W. Zhong, S. Liu, T. Gao, Z. Zhang, L. Xu, B. Song, 2D Transition Metal Dichalcogenides: Design, Modulation, and Challenges in Electrocatalysis, *Adv. Mater.* 33 (2021) 1907818.
- [19] D. Voiry, J. Yang, M. Chhowalla, Recent Strategies for Improving the Catalytic Activity of 2D TMD Nanosheets Toward the Hydrogen Evolution Reaction, *Adv. Mater.* 28 (2016) 6197–6206.
- [20] M. Chhowalla, H.S. Shin, G. Eda, L.J. Li, K.P. Loh, H. Zhang, The chemistry of two-dimensional layered transition metal dichalcogenide nanosheets, *Nat. Chem.* 5 (2013) 263–275.
- [21] C. Mattevi, M.S. Sokolikova, Direct synthesis of metastable phases of 2D transition metal dichalcogenides, *Chem. Soc. Rev.* 49 (2020) 3952–3980.
- [22] D. Voiry, H.S. Shin, K.P. Loh, M. Chhowalla, Low-dimensional catalysts for hydrogen evolution and CO₂ reduction, *Nat. Rev. Chem.* 2 (2018) 0105.
- [23] X. Chia, M. Pumera, Characteristics and performance of two-dimensional materials for electrocatalysis, *Nat. Catal.* 1 (2018) 909–921.
- [24] S. Guo, Y. Li, S. Tang, Y. Zhang, X. Li, A.J. Sobrido, M.M. Titirici, B. Wei, Monitoring Hydrogen Evolution Reaction Intermediates of Transition Metal Dichalcogenides via Operando Raman Spectroscopy, *Adv. Funct. Mater.* 30 (2020) 2003035.
- [25] Y. Zhou, J. Zhang, E. Song, J. Lin, J. Zhou, K. Suenaga, W. Zhou, Z. Liu, J. Liu, J. Lou, H.J. Fan, Enhanced performance of in-plane transition metal dichalcogenides monolayers by configuring local atomic structures, *Nat. Commun.* 11 (2020) 2253.
- [26] S. Padmajan Sasikala, Y. Singh, L. Bing, T. Yun, S.H. Koo, Y. Jung, S.O. Kim, Longitudinal unzipping of 2D transition metal dichalcogenides, *Nat. Commun.* 11 (2020) 5032.
- [27] J. Deng, H. Li, J. Xiao, Y. Tu, D. Deng, H. Yang, H. Tian, J. Li, P. Ren, X. Bao, Triggering the electrocatalytic hydrogen evolution activity of the inert two-dimensional MoS₂ surface via single-atom metal doping, *Energy Environ. Sci.* 8 (2015) 1594–1601.

- [28] Y. Shi, Y. Zhou, D.R. Yang, W.X. Xu, C. Wang, F. Bin Wang, J.J. Xu, X.H. Xia, H.Y. Chen, Energy Level Engineering of MoS₂ by Transition-Metal Doping for Accelerating Hydrogen Evolution Reaction, *J. Am. Chem. Soc.* 139 (2017) 15479–15485.
- [29] M.E. Pam, J. Hu, Y.S. Ang, S. Huang, D. Kong, Y. Shi, X. Zhao, D. Geng, S.J. Pennycook, L.K. Ang, H.Y. Yang, High-Concentration Niobium-Substituted WS₂ Basal Domains with Reconfigured Electronic Band Structure for Hydrogen Evolution Reaction, *ACS Appl. Mater. Interfaces.* 11 (2019) 34862–34868.
- [30] Y. Li, Q. Gu, B. Johannessen, Z. Zheng, C. Li, Y. Luo, Z. Zhang, Q. Zhang, H. Fan, W. Luo, B. Liu, S. Dou, H. Liu, Synergistic Pt doping and phase conversion engineering in two-dimensional MoS₂ for efficient hydrogen evolution, *Nano Energy.* 84 (2021) 105898.
- [31] Z. Luo, Y. Ouyang, H. Zhang, M. Xiao, J. Ge, Z. Jiang, J. Wang, D. Tang, X. Cao, C. Liu, W. Xing, Chemically activating MoS₂ via spontaneous atomic palladium interfacial doping towards efficient hydrogen evolution, *Nat. Commun.* 9 (2018) 2120.
- [32] D.C. Nguyen, T.L. Luyen Doan, S. Prabhakaran, D.T. Tran, D.H. Kim, J.H. Lee, N.H. Kim, Hierarchical Co and Nb dual-doped MoS₂ nanosheets shelled micro-TiO₂ hollow spheres as effective multifunctional electrocatalysts for HER, OER, and ORR, *Nano Energy.* 82 (2021) 105750.
- [33] P. Liu, J. Zhu, J. Zhang, K. Tao, D. Gao, P. Xi, Active basal plane catalytic activity and conductivity in Zn doped MoS₂ nanosheets for efficient hydrogen evolution, *Electrochim. Acta.* 260 (2018) 24–30.
- [34] A. Jain, M.B. Sadan, A. Ramasubramaniam, Promoting Active Sites for Hydrogen Evolution in MoSe₂ Transition-Metal Doping, *J. Phys. Chem. C.* 124 (2020) 12324–12336.
- [35] D. Vikraman, S. Hussain, K. Akbar, K. Karuppasamy, S.H. Chun, J. Jung, H.S. Kim, Design of Basal Plane Edges in Metal-Doped Nanostripes-Structured MoSe₂ Atomic Layers to Enhance Hydrogen Evolution Reaction Activity, *ACS Sustain. Chem. Eng.* 7 (2019) 458–469.
- [36] J. Qian, T. Wang, B. Xia, P. Xi, D. Gao, Zn-doped MoSe₂ nanosheets as high-performance electrocatalysts for hydrogen evolution reaction in acid media, *Electrochim. Acta.* 296 (2019) 701–708.
- [37] J. Zhang, J. Wu, H. Guo, W. Chen, J. Yuan, U. Martinez, G. Gupta, A. Mohite, P.M. Ajayan, J. Lou, Unveiling Active Sites for the Hydrogen Evolution Reaction on Monolayer MoS₂, *Adv. Mater.* 29 (2017) 1701955.
- [38] J. Zhu, Z.C. Wang, H. Dai, Q. Wang, R. Yang, H. Yu, M. Liao, J. Zhang, W. Chen, Z. Wei, N. Li, L. Du, D. Shi, W. Wang, L. Zhang, Y. Jiang, G. Zhang, Boundary activated hydrogen evolution reaction on monolayer MoS₂, *Nat. Commun.* 10 (2019) 1348.
- [39] J. Shi, D. Ma, G.F. Han, Y. Zhang, Q. Ji, T. Gao, J. Sun, X. Song, C. Li, Y. Zhang, X.Y. Lang, Y. Zhang, Z. Liu, Controllable growth and transfer of monolayer MoS₂ on Au foils and its potential application in hydrogen evolution reaction, *ACS Nano.* 8 (2014) 10196–10204.

- [40] X. Hai, W. Zhou, S. Wang, H. Pang, K. Chang, F. Ichihara, J. Ye, Rational design of freestanding MoS₂ monolayers for hydrogen evolution reaction, *Nano Energy*. 39 (2017) 409–417.
- [41] S. Bolar, S. Shit, J.S. Kumar, N.C. Murmu, R.S. Ganesh, H. Inokawa, T. Kuila, Optimization of active surface area of flower like MoS₂ using V-doping towards enhanced hydrogen evolution reaction in acidic and basic medium, *Appl. Catal. B Environ.* 254 (2019) 432–442.
- [42] B. Gao, X. Du, Y. Li, S. Ding, C. Xiao, Z. Song, Deep Phase Transition of MoS₂ for Excellent Hydrogen Evolution Reaction by a Facile C-Doping Strategy, *ACS Appl. Mater. Interfaces*. 12 (2020) 877–885.
- [43] S. Deng, M. Luo, C. Ai, Y. Zhang, B. Liu, L. Huang, Z. Jiang, Q. Zhang, L. Gu, S. Lin, X. Wang, L. Yu, J. Wen, J. Wang, G. Pan, X. Xia, J. Tu, Synergistic Doping and Intercalation: Realizing Deep Phase Modulation on MoS₂ Arrays for High-Efficiency Hydrogen Evolution Reaction, *Angew. Chemie - Int. Ed.* 58 (2019) 16289–16296.
- [44] L. Pei, H. Qiao, B. Chen, X. Zhu, R.A. Davis, K. Zhu, L. Xia, P. Dong, M. Ye, J. Shen, Pt edge-doped MoS₂ : Activating the Active Sites for Maximized Hydrogen Evolution, *Small*. 17 (2021) 2104245.
- [45] X. Zhang, F. Zhou, S. Zhang, Y. Liang, R. Wang, Engineering MoS₂ Basal Planes for Hydrogen Evolution via Synergistic Ruthenium Doping and Nanocarbon Hybridization, *Adv. Sci.* 6 (2019) 1900090.
- [46] G. Kresse, J. Furthmüller, Efficient iterative schemes for *ab initio* total-energy calculations using a plane-wave basis set, *Phys. Rev. B*. 54 (1996) 11169–11186.
- [47] J.P. Perdew, K. Burke, M. Ernzerhof, Generalized gradient approximation made simple, *Phys. Rev. Lett.* 77 (1996) 3865–3868.
- [48] P.E. Blöchl, Projector augmented-wave method, *Phys. Rev. B*. 50 (1994) 17953–17979.
- [49] Y.-H. Lee, X.-Q. Zhang, W. Zhang, M.-T. Chang, C.-T. Lin, K.-D. Chang, Y.-C. Yu, J.T.-W. Wang, C.-S. Chang, L.-J. Li, T.-W. Lin, Synthesis of Large-Area MoS₂ Atomic Layers with Chemical Vapor Deposition, *Adv. Mater.* 24 (2012) 2320–2325.
- [50] S. Barja, S. Wickenburg, Z.F. Liu, Y. Zhang, H. Ryu, M.M. Ugeda, Z. Hussain, Z.X. Shen, S.K. Mo, E. Wong, M.B. Salmeron, F. Wang, M.F. Crommie, D.F. Ogletree, J.B. Neaton, A. Weber-Bargioni, Charge density wave order in 1D mirror twin boundaries of single-layer MoSe₂, *Nat. Phys.* 12 (2016) 751–756.
- [51] Y. Wang, J. Xiao, H. Zhu, Y. Li, Y. Alsaïd, K.Y. Fong, Y. Zhou, S. Wang, W. Shi, Y. Wang, A. Zettl, E.J. Reed, X. Zhang, Structural phase transition in monolayer MoTe₂ driven by electrostatic doping, *Nature*. 550 (2017) 487–491.
- [52] J.A. Reyes-Retana, F. Cervantes-Sodi, Spin-orbital effects in metal-dichalcogenide semiconducting monolayers, *Sci. Rep.* 6 (2016) 24093.
- [53] Y. Qu, H. Pan, C.T. Kwok, Hydrogenation-controlled phase transition on two-dimensional transition metal dichalcogenides and their unique physical and catalytic properties, *Sci. Rep.* 6 (2016) 34186.

- [54] V.T. Nguyen, T.Y. Yang, P.A. Le, P.J. Yen, Y.L. Chueh, K.H. Wei, New Simultaneous Exfoliation and Doping Process for Generating MX₂ Nanosheets for Electrocatalytic Hydrogen Evolution Reaction, *ACS Appl. Mater. Interfaces*. 11 (2019) 14786–14795.
- [55] D. Vikraman, S. Hussain, K. Akbar, K. Karuppasamy, S.H. Chun, J. Jung, H.S. Kim, Design of Basal Plane Edges in Metal-Doped Nanostripes-Structured MoSe₂ Atomic Layers to Enhance Hydrogen Evolution Reaction Activity, *ACS Sustain. Chem. Eng.* 7 (2019) 458–469.
- [56] S.H. Mir, S. Chakraborty, J. Wärnå, S. Narayan, P.C. Jha, P.K. Jha, R. Ahuja, A comparative study of hydrogen evolution reaction on pseudo-monolayer WS₂ and PtS₂: Insights based on the density functional theory, *Catal. Sci. Technol.* 7 (2017) 687–692.
- [57] G. Henkelman, A. Arnaldsson, H. Jónsson, A fast and robust algorithm for Bader decomposition of charge density, *Comput. Mater. Sci.* 36 (2006) 354–360.
- [58] A. Bala, V. Kumar, Stability of the Eu²⁺ Dopant in CsPbBr₃ Perovskites: A First-Principles Study, *J. Phys. Chem. C*. 123 (2019) 6965–6969.
- [59] K. Momma, F. Izumi, VESTA 3 for three-dimensional visualization of crystal, volumetric and morphology data, *J. Appl. Crystallogr.* 44 (2011) 1272–1276.
- [60] D. Vikraman, S. Hussain, K. Karuppasamy, A. Kathalingam, E.B. Jo, A. Sanmugam, J. Jung, H.S. Kim, Engineering the active sites tuned MoS₂ nanoarray structures by transition metal doping for hydrogen evolution and supercapacitor applications, *J. Alloys Compd.* 893 (2022) 162271.
- [61] T.H.M. Lau, X. Lu, J. Kulhavy, S. Wu, L. Lu, T.S. Wu, R. Kato, J.S. Foord, Y.L. Soo, K. Suenaga, S.C.E. Tsang, Transition metal atom doping of the basal plane of MoS₂ monolayer nanosheets for electrochemical hydrogen evolution, *Chem. Sci.* 9 (2018) 4769–4776.
- [62] N. Xuan, J. Chen, J. Shi, Y. Yue, P. Zhuang, K. Ba, Y. Sun, J. Shen, Y. Liu, B. Ge, Z. Sun, Single-Atom Electroplating on Two Dimensional Materials, *Chem. Mater.* 31 (2019) 429–435.
- [63] A. Hasani, T.P. Nguyen, M. Tekalgne, Q. Van Le, K.S. Choi, T.H. Lee, T. Jung Park, H.W. Jang, S.Y. Kim, The role of metal dopants in WS₂ nanoflowers in enhancing the hydrogen evolution reaction, *Appl. Catal. A Gen.* 567 (2018) 73–79.
- [64] M. Kang, C. Lin, H. Yang, Y. Guo, L. Liu, T. Xue, Y. Liu, Y. Gong, Z. Zhao, T. Zhai, K. Zhai, A. Nie, Y. Cheng, Z. Liu, Proximity Enhanced Hydrogen Evolution Reactivity of Substitutional Doped Monolayer WS₂, *ACS Appl. Mater. Interfaces*. (2021) 19406–19413.
- [65] R. Liu, H.L. Fei, G.L. Ye, Recent advances in single metal atom-doped MoS₂ as catalysts for hydrogen evolution reaction, *Tungsten*. 2 (2020) 147–161.
- [66] W. Yang, S. Zhang, Q. Chen, C. Zhang, Y. Wei, H. Jiang, Y. Lin, M. Zhao, Q. He, X. Wang, Y. Du, L. Song, S. Yang, A. Nie, X. Zou, Y. Gong, Conversion of Intercalated MoO₃ to Multi-Heteroatoms-Doped MoS₂ with High Hydrogen.pdf, *Adv. Mater.* 32 (2020) 2001167.

- [67] J. Wang, W. Fang, Y. Hu, Y. Zhang, J. Dang, Y. Wu, B. Chen, H. Zhao, Z. Li, Single atom Ru doping 2H-MoS₂ as highly efficient hydrogen evolution reaction electrocatalyst in a wide pH range, *Appl. Catal. B Environ.* 298 (2021) 120490.
- [68] D. Er, H. Ye, N.C. Frey, H. Kumar, J. Lou, V.B. Shenoy, Prediction of Enhanced Catalytic Activity for Hydrogen Evolution Reaction in Janus Transition Metal Dichalcogenides, *Nano Lett.* 18 (2018) 3943–3949.
- [69] X. Sun, Z. Wang, Z. Li, Y.Q. Fu, Origin of Structural Transformation in Mono-and Bi-Layered Molybdenum Disulfide, *Sci. Rep.* 6 (2016) 26666.
- [70] M. Samadi, N. Sarikhani, M. Zirak, H. Zhang, H.L. Zhang, A.Z. Moshfegh, Group 6 transition metal dichalcogenide nanomaterials: Synthesis, applications and future perspectives, *Nanoscale Horizons.* 3 (2018) 90–204.
- [71] R. Luo, M. Luo, Z. Wang, P. Liu, S. Song, X. Wang, M. Chen, The atomic origin of nickel-doping-induced catalytic enhancement in MoS₂ for electrochemical hydrogen production, *Nanoscale.* 11 (2019) 7123–7128.
- [72] S. Fu, K. Kang, K. Shayan, A. Yoshimura, S. Dadras, X. Wang, L. Zhang, S. Chen, N. Liu, A. Jindal, X. Li, A.N. Pasupathy, A.N. Vamivakas, V. Meunier, S. Strauf, E.H. Yang, Enabling room temperature ferromagnetism in monolayer MoS₂ via in situ iron-doping, *Nat. Commun.* 11 (2020) 2034.
- [73] K.Y. Kim, J. Lee, S. Kang, Y.W. Son, H.W. Jang, Y. Kang, S. Han, Role of Hyper-Reduced States in Hydrogen Evolution Reaction at Sulfur Vacancy in MoS₂, *ACS Catal.* 8 (2018) 4508–4515.
- [74] H. Li, C. Tsai, A.L. Koh, L. Cai, A.W. Contryman, A.H. Fragapane, J. Zhao, H.S. Han, H.C. Manoharan, F. Abild-Pedersen, J.K. Nørskov, X. Zheng, Activating and optimizing MoS₂ basal planes for hydrogen evolution through the formation of strained sulphur vacancies, *Nat. Mater.* 15 (2016) 364.
- [75] J. Lee, C. Kim, K. Choi, J. Seo, Y. Choi, W. Choi, Y. Kim, H. Young, J. Hee, G. Kim, H. Park, Nano Energy In-situ coalesced vacancies on MoSe₂ mimicking noble metal: Unprecedented Tafel reaction in hydrogen evolution, *Nano Energy.* 63 (2019) 103846.
- [76] X. Wang, Y. Zhang, H. Si, Q. Zhang, J. Wu, L. Gao, X. Wei, Y. Sun, Q. Liao, Z. Zhang, K. Ammarah, L. Gu, Z. Kang, Y. Zhang, Single-Atom Vacancy Defect to Trigger High-Efficiency Hydrogen Evolution of MoS₂, *J. Am. Chem. Soc.* 142 (2020) 4298–4308.
- [77] Q. Tang, Tuning the phase stability of Mo-based TMD monolayers through coupled vacancy defects and lattice strain, *J. Mater. Chem. C.* 6 (2018) 9561–9568.
- [78] S. Wang, G. Do Lee, S. Lee, E. Yoon, J.H. Warner, Detailed Atomic Reconstruction of Extended Line Defects in Monolayer MoS₂, *ACS Nano.* 10 (2016) 5419–5430.
- [79] T. Vogl, K. Sripathy, A. Sharma, P. Reddy, J. Sullivan, J.R. Machacek, L. Zhang, F. Karouta, B.C. Buchler, M.W. Doherty, Y. Lu, P.K. Lam, Radiation tolerance of two-dimensional material-based devices for space applications, *Nat. Commun.* 10 (2019) 1202.
- [80] B. Huang, F. Tian, Y. Shen, M. Zheng, Y. Zhao, J. Wu, Y. Liu, S.J. Pennycook, J.T.L.

Thong, Selective Engineering of Chalcogen Defects in MoS₂ by Low-Energy Helium Plasma, ACS Appl. Mater. Interfaces. 11 (2019) 24404–24411.